Article

Molecular Cell

Terminal Uridylyltransferases Execute Programmed Clearance of Maternal Transcriptome in Vertebrate Embryos

Graphical Abstract

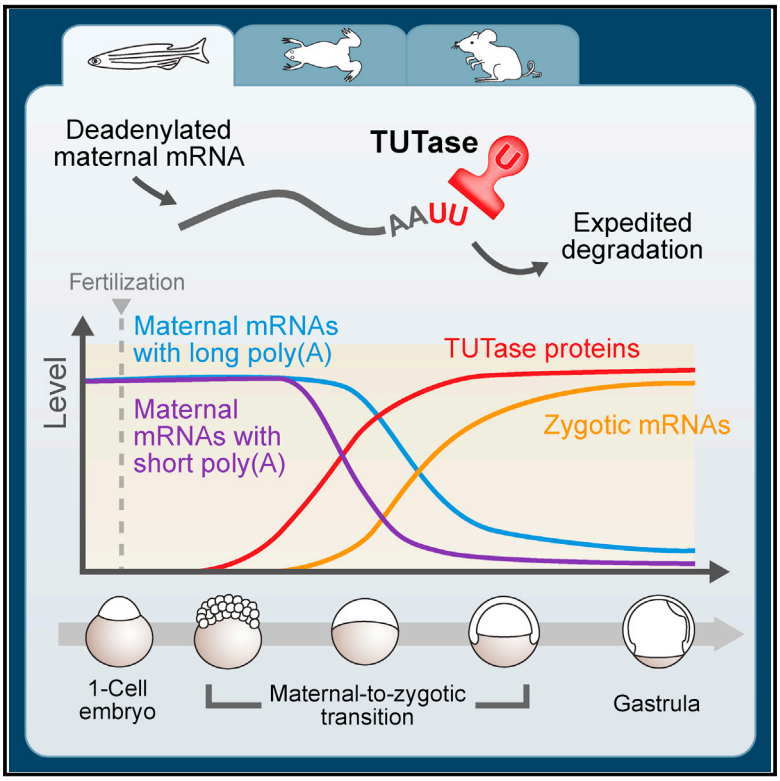

Authors

Hyeshik Chang, Jinah Yeo, Jeong-gyun Kim, ..., Hosung Jung, Kyu-Won Kim, V. Narry Kim

Correspondence

narrykim@snu.ac.kr

In Brief

An embryo begins its life with maternally deposited RNAs that undergo timely translation and degradation. Chang et al. show that terminal uridylyltransferases add uridine tails to trigger decay of short poly(A)-tailed RNAs and that uridylation is critical for temporal organization of transcriptome in early vertebrate embryos.

Highlights

- TUT4 and TUT7 are conserved writers of U tail in vertebrates
- mRNA uridylation is induced during early embryogenesis
- Uridylation facilitates the programmed elimination of maternal RNAs
- TUT4 and TUT7 are required for gastrulation in zebrafish and *Xenopus*

Chang et al., 2018, Molecular Cell *70*, 72–82
April 5, 2018
https://doi.org/10.1016/j.molcel.2018.03.004

CellPress

CellPress

Molecular Cell
Article

Terminal Uridylyltransferases Execute Programmed Clearance of Maternal Transcriptome in Vertebrate Embryos

Hyeshik Chang,[1,5] Jinah Yeo,[1,5] Jeong-gyun Kim,[2] Hyunjoon Kim,[1] Jaechul Lim,[1,3] Mihye Lee,[1] Hyun Ho Kim,[2] Jiyeon Ohk,[4] Hee-Yeon Jeon,[3] Hyunsook Lee,[3] Hosung Jung,[4] Kyu-Won Kim,[2] and V. Narry Kim[1,3,6,*]

[1]Center for RNA Research, Institute for Basic Science, Seoul 08826, Korea
[2]Department of Molecular Medicine and Biopharmaceutical Science, Seoul National University, Seoul 08826, Korea
[3]School of Biological Sciences, Seoul National University, Seoul 08826, Korea
[4]Department of Anatomy, Yonsei University College of Medicine, Seoul 03722, Korea
[5]These authors contributed equally
[6]Lead Contact
*Correspondence: narrykim@snu.ac.kr
https://doi.org/10.1016/j.molcel.2018.03.004

SUMMARY

During the maternal-to-zygotic transition (MZT), maternal RNAs are actively degraded and replaced by newly synthesized zygotic transcripts in a highly coordinated manner. However, it remains largely unknown how maternal mRNA decay is triggered in early vertebrate embryos. Here, through genome-wide profiling of RNA abundance and 3′ modification, we show that uridylation is induced at the onset of maternal mRNA clearance. The temporal control of uridylation is conserved in vertebrates. When the homologs of terminal uridylyltransferases TUT4 and TUT7 (TUT4/7) are depleted in zebrafish and *Xenopus*, maternal mRNA clearance is significantly delayed, leading to developmental defects during gastrulation. Short-tailed mRNAs are selectively uridylated by TUT4/7, with the highly uridylated transcripts degraded faster during the MZT than those with unmodified poly(A) tails. Our study demonstrates that uridylation plays a crucial role in timely mRNA degradation, thereby allowing the progression of early development.

INTRODUCTION

Maternal-to-zygotic transition (MZT) constitutes one of the most dramatic reprogramming processes in animal development, in which a highly differentiated egg is converted into a totipotent embryo, resetting the developmental clock. Because an early embryo is transcriptionally silenced, the initial events of embryonic reprogramming are driven by maternal factors (Tadros and Lipshitz, 2009; Yartseva and Giraldez, 2015). Most maternal transcripts are deposited with short poly(A) tails in an oocyte, with their polyadenylation being a crucial event to embark the first wave of protein synthesis in an embryo (Weill et al., 2012). During this first wave of translation, some essential factors for zygotic genome activation are produced, including pioneering transcription factors such as Nanog, Pou5f3 (a homolog of human Oct4), and SoxB1 (Lee et al., 2013). Another critical event during early embryogenesis is the timely removal of maternal mRNAs, which allows the subsequent developmental transition to proceed (Walser and Lipshitz, 2011). Both maternal and zygotic pathways contribute to the deadenylation and decay of maternal transcripts. Several factors have been identified in these pathways (Yartseva and Giraldez, 2015). For example, in zebrafish and mouse, maternally supplied N^6-methyladenosine (m6A) reader Ythdf2 promotes deadenylation of a subset of maternal mRNAs (Ivanova et al., 2017; Zhao et al., 2017). Suboptimal codon usage also affects RNA stability by accelerating deadenylation via the maternal decay pathway (Bazzini et al., 2016; Mishima and Tomari, 2016). In turn, the zygotic decay pathway is in part mediated by miR-430, which triggers the deadenylation of cognate transcripts (Bazzini et al., 2012; Giraldez et al., 2006). However, these deadenylation factors account for only a subset of maternal mRNA clearance; it remains unknown which factors act in the steps following deadenylation.

Poly(A) tails and oligo(U) tails comprise key players in mRNA stability control (Lim et al., 2014; Scott and Norbury, 2013). Approaching the end of an mRNA life cycle, the poly(A) tail is shortened by deadenylases, which leads to dissociation of poly(A)-binding proteins (PABPs) from the tail. We previously reported that, in human cells, two closely related terminal uridylyltransferases (TUT4 and TUT7) target PABP-free RNAs with short (A) tails (approximately <20 nt) for 3′ end uridylation (Lim et al., 2014). Uridylation is thought to facilitate both 5′-to-3′ and 3′-to-5′ decay pathways for the rapid elimination of deadenylated mRNAs (Lim et al., 2014). TUT4/7-mediated mRNA uridylation has recently been implicated in the clearance of mRNAs during oocyte growth in mice (Morgan et al., 2017). Poly(A)+ mRNA uridylation was also observed in *Schizosaccharomyces pombe* (Rissland et al., 2007), *Aspergillus nidulans* (Morozov et al., 2012), *Patiria pectinifera* (Ochi and Chiba, 2016), and *Arabidopsis thaliana* (Sement et al., 2013), suggesting the fundamental and diverse roles of uridylation across eukaryotes.

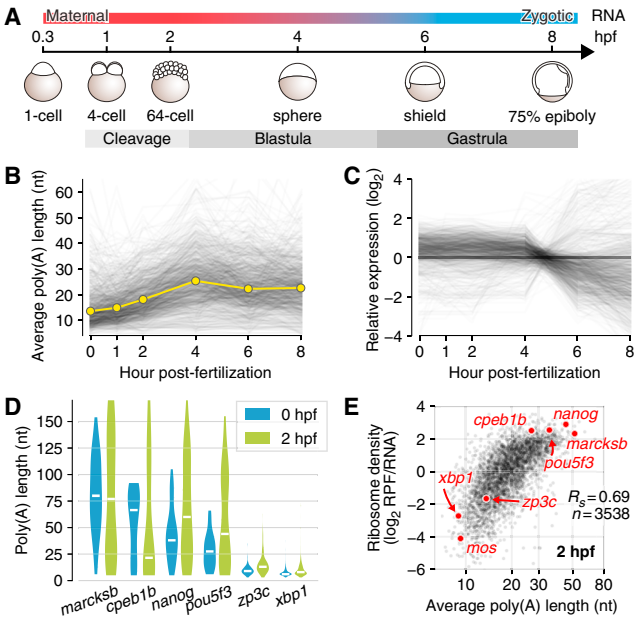

Figure 1. Temporal Profiles of mRNA Tails in the Zebrafish MZT

(A) Illustration of the zebrafish developmental stages examined by TAIL-seq. Transcription starts after the 64-cell stage. The majority of MZT events take place between 2 and 6 hpf.

(B) Average poly(A) tail length of individual genes (geometric means of poly(A) lengths ≥5 nt). The yellow line represents the median for all genes with at least 100 reads per million (RPM) mapped tags in any sample.

(C) Relative RNA levels of genes shown in (B), which were normalized using the geometric mean of RPMs.

(D) Violin plot for poly(A) length distributions of six genes at 0 and 2 hpf zebrafish embryos. The white horizontal bars show the median lengths of poly(A) tails ≥5 nt.

(E) Associations between poly(A) length and ribosome density at 2 hpf. Each dot shows an mRNA that encodes a non-histone protein and has ≥30 tags in our TAIL-seq data.

See also Figure S1.

In this study, we investigated the regulation and function of mRNA tails in animal embryos. We find that mRNA tails, particularly U tails, are dynamically controlled and that loss of U tails leads to developmental defects. Our results unveil a pivotal role of uridylation in the progression of early vertebrate development.

RESULTS

TAIL-Seq Reveals Transcriptome Dynamics in the Zebrafish MZT

To understand how the mRNA tail is regulated during the vertebrate MZT, we performed tail sequencing (TAIL-seq) on zebrafish embryos (Figure 1A). Briefly, mRNAs were enriched by size fractionation (approximately >200 nt) and rRNA depletion and were ligated to the 3′ adaptor that contains biotin residues. After partial digestion, the 3′ fragments were purified with streptavidin beads and were ligated to the 5′ adaptor for amplification and sequencing (Chang et al., 2014). The overall profile of poly(A) tail length confirms previous notions that maternal mRNAs undergo global polyadenylation during early embryogenesis (Figures 1B and S1A). The tails of maternally deposited mRNAs are short (median length, 13.5 nt) in fertilized eggs at 0 hours post-fertilization (hpf). During the cleavage stage (1–2 hpf), mRNA tails gradually elongate to reach 18.1 nt (median) (Figure 1B). By the blastula stage (4 hpf), poly(A) tail length further increases to 25.4 nt (median). At this stage, much longer tails of 50–150 nt are also observed depending on the respective genes (Figure S1A), owing to zygotic *de novo* transcription which begins at approximately 3 hpf (Harvey et al., 2013; Heyn et al., 2014).

Contrary to these dynamic changes in the tail length, our data indicated that the abundance of most mRNAs remains constant during the first 4 hr (Figures 1C and S1B). Thus, the decay machinery is set to act mainly after 4 hpf although a minor fraction of maternal transcripts begins to be degraded earlier (2–4 hpf; "early decay" genes; cluster *a* in Figure S1B). The majority of maternal transcripts are deadenylated and degraded rapidly between 4 and 6 hpf, concurrently with the major zygotic transcription period. Out of 3,476 genes detected in our TAIL-seq dataset, 1,611 (46.3%) maternally provided transcripts phase out before 6 hpf.

Closer examination of TAIL-seq data revealed substantial variations of the poly(A) tail length among genes. Although most transcripts harbor short tails in the pre-MZT embryos at 0 hpf, 9.7% of the detected genes are deposited with long poly(A) tails (>30 nt on average). Genes with a function in either calmodulin binding (median length = 35.5; $p < 0.0012$) or mRNA 3′ UTR binding (median length = 33.7; $p < 0.00085$) have particularly long poly(A) tails. The calmodulin-binding proteins are regulated by calcium waves in the earliest cell cycles and play important roles in early development (Webb and Miller, 2000). For example, Marcks proteins, which are involved in gastrulation and neural development (Ott et al., 2011; Prieto and Zolessi, 2017), are encoded by transcripts with long poly(A) tails (69.9 and 37.9 nt for *marcksb* and *marcksa*, respectively). Some 3′ UTR binding proteins also have long tails (40.2, 42.2, and 39.7 nt for *cpeb1b*, *cth1*, *and cirbpa*, respectively), which implies that they may be translated prior to the MZT and bootstrap the transcriptome to control their fates in later stages. Also notable are the *nanog* and *pou5f3* mRNAs that harbor substantially longer tails than others (*zp3c* and *xbp1*) (Figure 1D). Consistent with previous reports from zebrafish and fly embryos (Eichhorn et al., 2016; Lim et al., 2016; Subtelny et al., 2014), there is an obvious correlation between the poly(A) length and translation efficiency before the MZT (Figure 1E), indicating that poly(A) tails have a strong impact on translation in the pre-MZT embryo. For example, the transcripts deposited with long poly(A) tails such as *nanog* are translationally induced at an earlier stage than transcripts with shorter tails. Thus, early embryos rely mainly on poly(A) tails to achieve temporal regulation of maternal protein synthesis, although additional gene-specific regulatory elements may also contribute.

U Tails Emerge at the Onset of the MZT in Vertebrates

In pre-MZT embryos, most mRNAs are stable even though they have unusually short poly(A) tails (Barckmann and Simonelig, 2013). This is in stark contrast to somatic cells where deadenylation generally leads to immediate degradation of mRNA body (Houseley and Tollervey, 2009). This apparent uncoupling between deadenylation and decay suggests that some

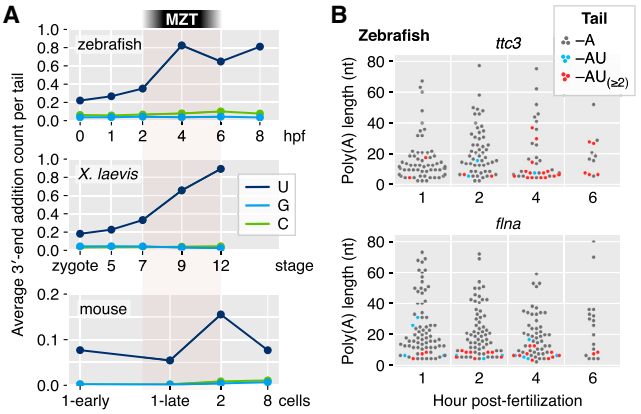

Figure 2. Developmental Regulation of Uridylation

(A) Average 3′ non-A nucleotide addition per tail, determined using all the mRNA reads containing 5–15 nt poly(A) tails. The light brown shadow roughly spans the MZT duration. *X. laevis* stages are indicated in the Nieuwkoop and Faber (NF) stage numbers.

(B) Poly(A) length and uridylation status of two representative genes. A dot represents a single sequence read. The color indicates the length of U at the 3′ end. The number of dots in any sample is proportional to the relative RNA abundance measured by RNA-seq.

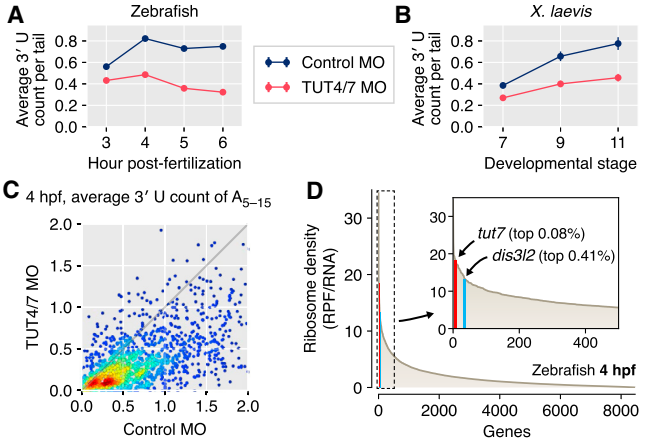

Figure 3. TUT4/7-Driven U Tailing of Poly(A) Tails

(A and B) Average uridylation count per tail, measured after the injection of control or TUT4/7 translation-blocking morpholino (MO) into zebrafish (A) or frog (B) embryos. y axis shows the arithmetic mean of gene-level average U counts in the short poly(A) tails (5–15 nt). In zebrafish experiments, all SEM of the average U counts were smaller than 0.012. SEM is shown as vertical bars in (B).

(C) Average uridylation count per tail (5–15 nt) in 4 hpf zebrafish embryos injected with control or TUT4/7 MOs. Each dot represents a gene with ≥10 short poly(A) tags in both samples. The color of a dot shows the density of dots nearby; blue (low), green-yellow (medium), or red (high).

(D) Ribosome density distribution of expressed genes in the 4 hpf zebrafish embryo. The curves show all non-histone coding genes with ≥20 reads by RNA-seq after trimmed mean of M-values (TMM) normalization. Genes *tut7* and *dis3l2* are indicated by red and blue vertical bars in both full (lower left) and zoomed-in (upper right) planes.

See also Figures S2–S4.

component(s) of mRNA degradation machinery may be suppressed or absent in pre-MZT embryos.

Notably, when we examined the 3′ end sequences of mRNAs in zebrafish, we discovered that uridylation frequency is very low in fertilized eggs (0 hpf), whereas it increases drastically at the beginning of the MZT (Figure 2A, upper; Figures 2B and S2A). Other terminal modifications (e.g., G and C tails) remain at low levels throughout embryogenesis. To examine whether the regulation of uridylation is conserved in other species, we performed TAIL-seq experiments on *Xenopus* and mouse embryos. Of note, for mouse, we had to adopt a modified protocol termed mTAIL-seq to analyze the small numbers of embryos. mTAIL-seq is more sensitive than TAIL-seq but underestimates the frequencies of non-A tails (Lim et al., 2016). As in zebrafish, uridylated poly(A) tails are uncommon in fertilized eggs but increases during the MZT in both frogs and mice (Figure 2A; middle and bottom). By analyzing *Xenopus* oocytes, we also found that uridylation increases during oocyte maturation but decreases upon egg activation (Figures S2B and S2C). Our data suggest that there may be at least two rounds of uridylation surge in development: first during oocyte maturation and second during the MZT. This is consistent with a recent report that oligouridylated transcripts increase during mouse oocyte development (Morgan et al., 2017). We further expanded the analysis to an invertebrate, *Drosophila.* In the fruit fly, uridylation frequency remains low and does not show significant changes throughout embryogenesis (Figure S2D). Thus, the developmental control of uridylation appears to prevail in vertebrates but not in invertebrates.

TUT4 and TUT7 Are Conserved "Writers" of U Tail in Vertebrates

Next, we identified the zebrafish and frog orthologs of terminal uridylyltransferases TUT4 and TUT7 (TUT4/7) both of which are highly conserved in vertebrates (Figure S3). We blocked their translation by injecting morpholinos (MOs) complementary to the start codon into 1-cell embryos and examined RNA tail profiles by TAIL-seq. In both zebrafish and *Xenopus* embryos, when the TUT4/7 production was blocked, the upregulation of uridylation during the MZT was abolished (Figures 3A–3C). We also observed that TUT4/7 knockdown partially blocks the increase of uridylation during *Xenopus* oocyte maturation (Figures S4A and S4B). Thus, TUT4 and/or TUT7 are responsible for mRNA uridylation in fish and frog, as well as in mammals (Lim et al., 2014; Morgan et al., 2017). Conversely, the splicing-blocking morpholinos had no detectable effect during these stages (data not shown), which is consistent with a previous report (Thornton et al., 2014). This indicates that the TUT4/7 proteins translated from maternal mRNAs, rather than those from zygotically synthesized mRNAs (which require splicing), are responsible for mRNA uridylation during the MZT. According to the ribosome profiling (ribo-seq) data (re-analyzed from Subtelny et al., 2014), TUT7 is one of the most efficiently translated proteins among those detected at 4 hpf in zebrafish (Figure 3D). In comparison, the translational activation of TUT4 is more gradual (data not shown). Knockdown of TUT4 did not have a significant effect on mRNA uridylation until the blastula stages (Figure S4C). Notably, Dis3l2, an exonuclease that specifically degrades oligo-uridylated RNA, is also actively translated from maternally

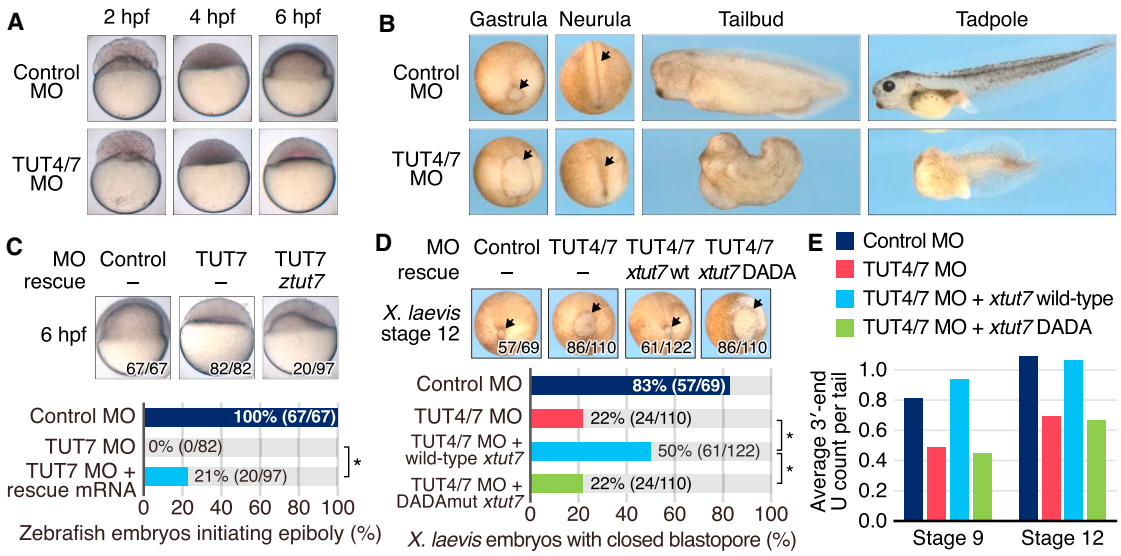

Figure 4. Morphological Defects by TUT4/7 Translation-Blocking Morpholinos

(A and B) Zebrafish (A) and frog (B) embryos showing the effects of TUT4/7 morpholinos (MOs). In (B), black arrows indicate the edges of the blastopore (gastrula) and the positions of neural tube closure (neurula).

(C) Zebrafish embryos displaying the rescue effects after co-injection of TUT7 morpholino and *tut7* mRNA. (top) Representative images of embryos injected with each treatment as annotated above. The numbers on the bottom right corner of each panel indicate the embryo count showing the same morphological characteristics as the presented image and the total number of embryos used for the experiment, respectively. (bottom) The number of embryos that progressed to the beginning of epiboly. An asterisk indicates a significant effect ($p < 1.17 \times 10^{-5}$; Fisher's exact test).

(D) Frog embryos demonstrating the rescue effect of the *tut7* mRNA injection. (top) The embryos were injected with control or TUT4/7 morpholino, along with GFP mRNA as a control (leftmost and the second), frog wild-type *tut7* mRNA (third), or frog *tut7* mRNA with a "DADA" mutation in its active site (rightmost). Black arrows indicate the positions of the blastopore. Numbers on the bottom right corner of each panel indicate the embryo counts with the shown morphology and total counts, respectively. (bottom) The number of embryos without defects in blastopore closure. An asterisk indicates a significant effect ($p < 1.15 \times 10^{-3}$; Fisher's exact test; two conditions resulted in the exactly same counts by chance).

(E) Average length of U tails per tail of all 5–15 nt poly(A) tails in frog stages 9 and 12.

See also Figure S5.

deposited mRNAs during the MZT (Figure 3D). In *X. laevis*, the orthologs of TUT7 and DIS3L2 accumulate during the midblastula transition at the most significant rates among the proteins related to RNA catabolism, according to the proteomic data by Peshkin et al. (2015) (Figure S4D). Thus, both the "writer" and a "reader" of the uridylation pathway are translationally induced during the MZT in vertebrates. These results suggest that TUT4/7 are the missing components of mRNA decay machinery and their translational induction restores the silenced RNA decay activity. It is also plausible that short poly(A) tails are actively protected from degradation and uridylation overrides this protection.

Uridylation Is Required for the Progression of Early Development

To understand the functional consequences of uridylation, we next examined the morphological phenotype (Figure 4). When TUT4/7 production was blocked in zebrafish, the transition from the sphere to shield stage was affected, displaying an early gastrulation defect (Figures 4A and S5A). Specifically, the zebrafish embryos fail to complete epiboly, which is a massive cell movement event during gastrulation. TUT7 single knockdown also resulted in a similar developmental arrest, whereas TUT4 morpholino (MO) caused a modest effect, possibly owing to a relatively low level of TUT4 (Figure S5A). The majority of TUT4 morphants were hardly distinguishable from control embryos until the shield stage (6 hpf), although they did not progress to the late epiboly stage. The severity of the morphological defect correlates with that of uridylation frequency (5 hpf; Figure S4C). The double knockdown yielded the most severe effects on both uridylation and development. Although the TUT4 single knockdown did not have a significant impact on uridylation, the double knockdown had a stronger effect than that of the TUT7 single knockdown, implicating some contribution of TUT4. Taken together, our results indicate that TUT7 may be the dominant enzyme in mRNA uridylation prior to gastrulation and that uridylation may be critically required for embryonic development in zebrafish.

Highly consistent results were obtained from *Xenopus* embryos. The TUT4/7 morphants exhibited typical gastrulation defects: failed blastopore closure and defective convergent extension (Figure 4B), which are equivalent to the gastrulation defects in zebrafish. Individual knockdown revealed that, as in zebrafish, TUT7 is required for the uridylation of mRNA (Figure S5B) as well as for the successful completion of gastrulation (Figure S5C). Knockdown of TUT4 did not have a detectable effect on either uridylation or development (Figures S5B and S5C). Multiple distinct morpholinos gave consistent results, whereas the control morpholino with mismatches did not impair developmental progression (Figure S5D).

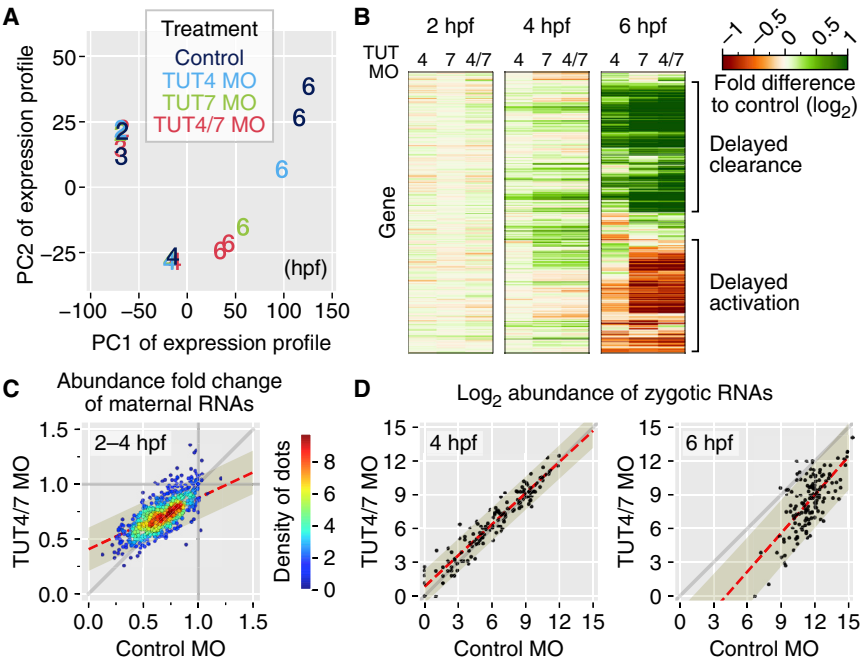

Figure 5. Effects of TUT4/7 Depletion on the Transcriptome Dynamics

(A) Principal component analysis summarizing transcriptome profiles at the given time points (digits, in hpf). The color indicates the morpholino injected to zebrafish embryos.

(B) Heatmaps showing the effects of TUT4/7 knockdown on RNA abundance. Each cell shows $\log_2$ fold ratio between RNA abundance in control and that in knockdown embryos. The numeric labels on the top of each column indicate the target(s) of the morpholino that is injected to the 1-cell embryo (4 for TUT4; 7 for TUT7; and 4/7 for TUT4/7).

(C) Fold change of RNA abundance between 2 and 4 hpf. The dots indicate genes from the "early decay" group with color indicating density of nearby dots. The red line and yellowish shade show the trend line and 95% prediction interval from linear regression, respectively.

(D) RNA levels of zygotic genes. A red broken line is the trend by linear regression. A yellow area covers the 95% prediction interval.

See also Figure S6.

To examine the possibility of off-target effects, we performed rescue experiments by co-injecting the *tut4* and *tut7* mRNAs that lack the morpholino-binding sites. Zebrafish *tut4* and *tut7* mRNAs could partially rescue the developmental defects of TUT4 and TUT7 morphants, respectively (Figures 4C and S5E). In *Xenopus*, we used catalytically dead mutant (DADA) as well as wild-type *tut7* for rescue experiments (Lapointe and Wickens, 2013). Wild-type *tut7* could recurrently restore gastrulation, whereas the DADA mutant showed no rescuing effect (Figure 4D), excluding the likelihood of off-target effects. We also measured the level of uridylation at stages 9 and 12. The TUT7 morphants showed a reduced level of uridylation, which could be reversed by wild-type *tut7* mRNA but not by the catalytic mutant (Figure 4E). Thus, the loss of uridylation activity is responsible for the developmental phenotypes observed in this study. Note that the let-7 microRNA (miRNA) family, well-known substrates of TUT4/7, is not detected until 8 hpf in zebrafish (Giraldez et al., 2006; Pasquinelli et al., 2000). So our observations for TUT4/7 phenotypes precede the induction of let-7 by a sufficient margin. Moreover, other miRNAs expressed at 4–6 hpf do not contain the sequences and structures required for TUT4/7-mediated regulation found in mammals (Heo et al., 2012; Kim et al., 2015), suggesting that the phenotypes of TUT4/7 knockdown observed in this study are independent of the miRNA pathway.

TUT4/7 Are Essential for the Transcriptome Remodeling during the MZT

To investigate whether and how the failure of uridylation affects the embryonic transcriptome, we performed RNA sequencing at 2, 3, 4, and 6 hpf following morpholino injection. The first principal component (PC1) of the gene expression profiles reflects the expected developmental status of the embryos (Figure 5A). In controls (Figure 5A, dark blue digits), the transcriptome at 4 hpf is distinct from that at 2–3 hpf, and the 4 hpf transcriptome differentiates further when the embryo reaches 6 hpf. In the TUT7 or TUT4/7 morphants (Figure 5A, green and red digits, respectively), PC1 at 6 hpf does not diverge from 4 hpf as much as in control embryos. This delay in transcriptomic remodeling accords with the aforementioned morphological phenotypes.

The gene-level analysis shows that the TUT7 or TUT4/7 knockdown results in a widespread delay of RNA decay even at 4 hpf albeit to a modest extent (Figure 5B, middle). This raises a question whether these changes are due directly to a defect in RNA degradation, or rather to the delayed activation of the zygotic genome. To address this issue, we first focused on the earliest changes induced by the TUT4/7 morpholinos at 2–4 hpf. During this early period, 25.3% of maternal transcripts decreased significantly in a TUT4/7-dependent manner (Figures S1B and 5B). The abundance of "early decay" group, whose members begin to decay after 2 hpf, decreased at a reduced rate (47% of the original rate) in TUT4/7 morphants compared to control embryos (Figure 5C). Meanwhile, the zygotic transcript levels were not affected by TUT4/7 knockdown at this time (Figures 5D, left), indicating that the first wave of zygotic transcription (which begins at 3 hpf) initiated normally. The zygotic transcriptome gets substantially disturbed only at 6 hpf in TUT4/7 morphants (Figure 5D, right). Consistent with this, several zygotic genes previously known as first-wave genes (i.e., *mapk12b*, *sox19a*, and *asb11*) are expressed at normal levels until 4 hpf in TUT4/7 morphants (Figure S6A), whereas the degradation of maternal transcripts such as *atp6v1*, *piwil2*, and *prkcda* is delayed as early as at 4 hpf (Figure S6B). Thus, the failure in maternal RNA decay precedes faulty zygotic transcription in TUT4/7 morphants.

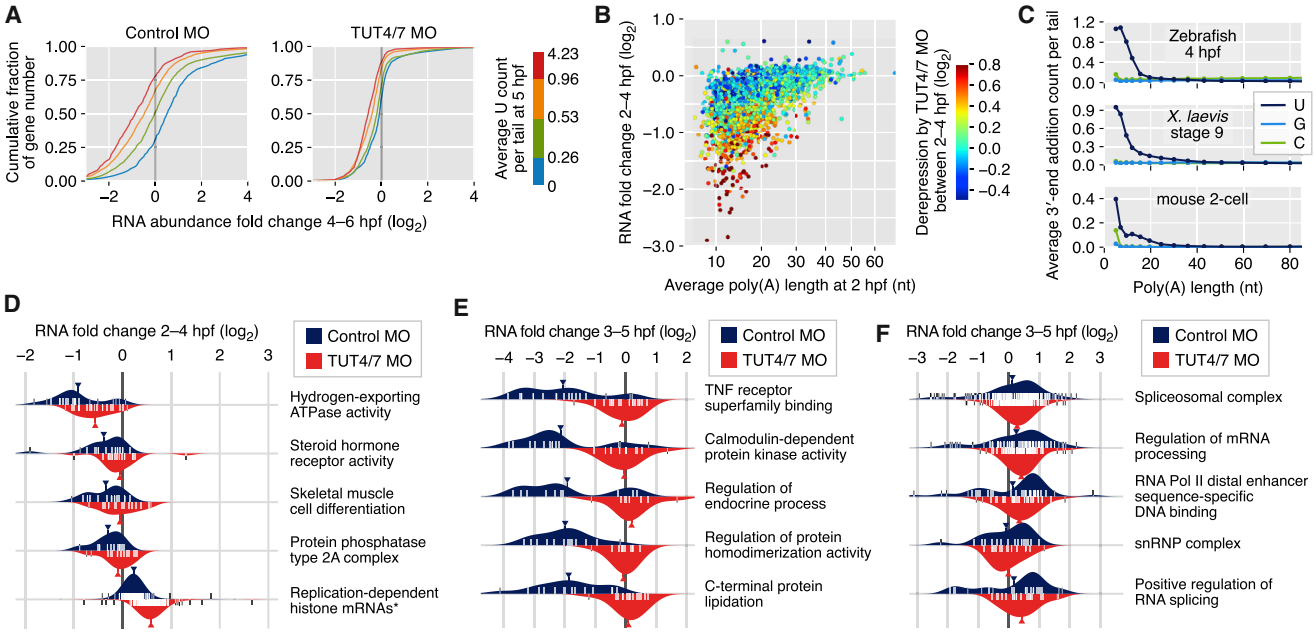

Figure 6. Molecular and Functional Consequences of TUT4/7's Substrate Selectivity

(A) Cumulative distribution plots for the RNA abundance changes between 4 and 6 hpf of four gene groups with different uridylation levels in control embryos at 5 hpf. The color bar on the right side shows the intervals of average U count per tail of 5–15 nt poly(A) tails of the gene groups.

(B) Association among poly(A) length at 2 hpf (x axis), RNA abundance change between 2–4 hpf (y axis), and the degree of derepression caused by TUT4/7 between 2–4 hpf (color). Derepression level is the difference between RNA abundance fold changes in controls and those in TUT4/7 morphants in 2–4 hpf. Each dot represents a single gene.

(C) Frequency of non-A tail at the 3′ end of poly(A) tail in vertebrate embryos around the time of maternal RNA decay activation.

(D–F) Gene ontology terms whose associated genes are most affected (D and E) or least (F) affected by the TUT4/7 knockdown. In each row, the upper side of the bean-shaped area shows RNA level changes in control embryos, whereas the lower side shows the distributions in TUT4/7 morpholino-treated embryos. The white vertical line indicates the change of each gene. The black line with a triangular end stands for the mean of the changes of genes in the gene set. See STAR Methods for the detailed procedures.

See also Figure S7.

U Tail Confers the Selectivity of RNA Decay during the MZT

To examine whether TUT4/7 indeed control maternal RNA decay, we compared the abundance changes and uridylation levels of maternal mRNAs (Figure 6A). Highly uridylated transcripts are downregulated to a greater degree than those that are less uridylated, demonstrating the tight association between uridylation and mRNA clearance (Figure 6A, left). Moreover, TUT4/7 knockdown alleviated the differences in decay rates (Figure 6A, right), which indicates that TUT4/7-mediated uridylation promotes mRNA decay.

To uncover the specificity of TUT4/7, we examined the poly(A) tail length of individual genes (at 2 hpf) and their subsequent abundance changes (2–4 hpf) (Figure 6B). This period (2–4 hpf) was chosen to avoid complex downstream effects and zygotic transcription. Notably, genes that are derepressed in TUT4/7 morphants (Figure 6B, red dots) are markedly enriched among the genes with short poly(A) tails (x axis) and those that are downregulated strongly between 2–4 hpf in control embryos (y axis). Consistent with these observations, an analysis of individual poly(A)+ tags showed that only short-tailed molecules are normally removed at 2–4 hpf (Figure S7A, columns 1 and 3), whereas they persist in the absence of TUT4/7 (Figure S7A, columns 1 and 2). Furthermore, the depletion of TUT4/7 causes the global accumulation of short poly(A) mRNAs (Figure S7B). These data clearly indicate that TUT4/7 selectively target deadenylated RNAs and facilitate their degradation. Consistent with this notion, uridylation is observed almost exclusively among deadenylated mRNAs in all species examined (fish, frog, and mouse embryos) (Figure 6C). Taken together, in vertebrate embryos, deadenylated mRNAs are selectively subject to rapid decay owing to the marked induction of TUT4/7 at the onset of the MZT.

Uridylation Promotes Temporally Organized Shaping of the Maternal Transcriptome

We next performed gene set enrichment analysis to uncover the gene ontology (GO) terms associated with the target genes of TUT4/7. During the first wave of maternal mRNA decay (2–4 hpf), in which the majority of transcriptomic changes are directly linked to TUT4/7 proteins (Figure 6D), strong enrichment was found in "steroid hormone receptor activity," which is critical for ovarian maturation (Vitti et al., 2016). These transcripts comprise the remnants from the late stages of oogenesis, which are carried over owing to the silenced RNA degradation pathways, and may thus need to be removed at the earliest stages of development. Also notable are the genes for

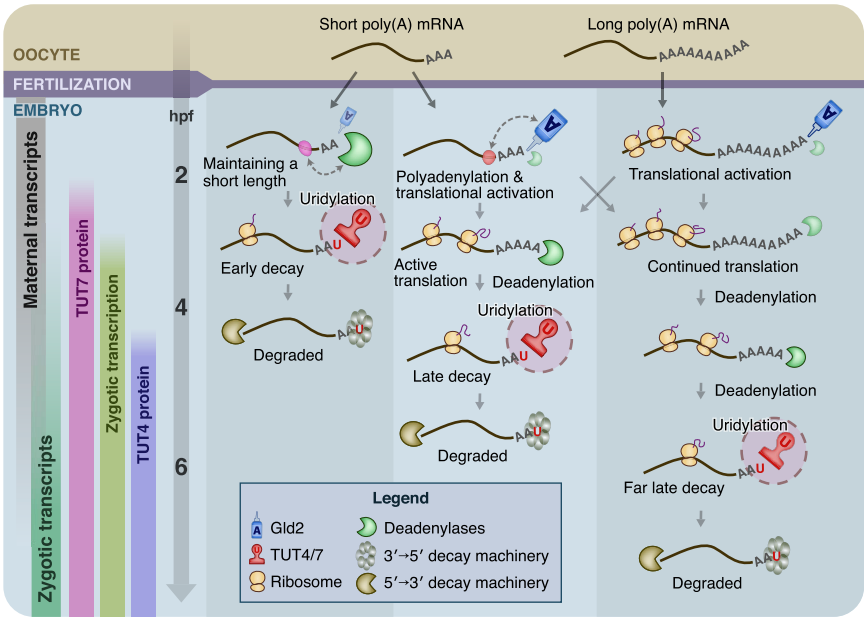

Figure 7. Schematic Model for Different Fates of Maternal RNAs via Tail-Mediated Regulation

Maternal mRNAs are deposited with different lengths of poly(A) tails (top). During the earliest cell cycles, poly(A) tails are differentially elongated depending on the interaction with cytoplasmic polyadenylase and deadenylases (the first row in the lower part). Once TUT7 protein is translated from maternally supplied mRNAs, shortened poly(A) tails (< approximately 15 nt) are uridylated and subjected to decay shortly after. An mRNA with a longer tail produces a required amount of protein products until it is committed for degradation by deadenylation and uridylation. Diverse mechanisms intensely control poly(A) tail length before and after fertilization to produce proteins with temporal and quantitative precision. TUT4/7-mediated uridylation promotes such tight regulation by committing deadenylated mRNAs to rapid degradation pathway.

"hydrogen-exporting ATPase activity." These genes are mostly involved in mitochondrial oxidative phosphorylation (OXPHOS), which is actively utilized during oocyte maturation (Van Blerkom, 2011). In vertebrates, mitochondrial copy number is known to increase dramatically during oocyte development but decrease during the early stages of embryonic development (Facucho-Oliveira and St John, 2009). Our data suggest that the OXPHOS pathway may be post-transcriptionally inactivated after fertilization via uridylation pathway (Figure S7C). Such dynamic regulation of mitochondrial biogenesis may reflect the vital need for metabolic remodeling in early embryogenesis and stem cell maintenance (Folmes et al., 2012).

We further found that some of the early induced zygotic transcripts accumulate to abnormally high levels in the TUT4/7 morphants, suggesting that they may also be subject to uridylation and rapid turnover. Most notably, replication-dependent histone mRNAs are significantly upregulated in the morphants (Figure 6D). In many animals including zebrafish, the initial cell cycles progress rapidly without gap phases, and zygotic histone mRNA levels oscillate over the cell cycle (Marzluff et al., 2008). It was previously shown that TUT4/7 uridylate histone mRNAs and enhance their decay at the end of S phase in human cells (Lackey et al., 2016; Mullen and Marzluff, 2008; Schmidt et al., 2011; Su et al., 2013). Our current data indicate that the function of TUT4/7 in histone mRNA decay is conserved and that TUT4/7 knockdown may distort the tight regulation of histones, which leads to disorganized development.

Approaching the end of the blastula period (approximately 5 hpf), full-scale maternal mRNA decay occurs, with the vast majority of gene sets being downregulated during the 3- to 5-hpf period (Figure S7D). TUT4/7 knockdown interrupts and delays the downregulation of most gene sets including "tumor necrosis factor (TNF) receptor binding," "calmodulin-dependent protein kinase activity," and "regulation of endocrine process" (Figures 6E and S7D), which may result in catastrophic disorganization of the regulatory network. At the other end of the spectrum, however, a relatively homogeneous group of gene sets, mostly related to RNA synthesis and splicing, remains constant during the MZT and is not affected by TUT4/7 knockdown (Figure 6F).

DISCUSSION

Our study introduces RNA uridylation as a key molecular event that triggers mRNA decay during the vertebrate MZT (modeled in Figure 7). Most maternal mRNAs are inherited with unusually short poly(A) tails. However, deadenylation and decay are uncoupled in eggs prior to MZT, allowing the short-tailed mRNAs to remain stably deposited (Duval et al., 1990; Su et al., 2007). Upon fertilization, TUT7 (and TUT4 to a more modest extent) are translated and act on short-tailed mRNAs. Oligo (U) tail is preferentially recognized by the LSM1–7 complex and the 3′-to-5′ exoribonuclease DIS3L2, which mediate decapping and decay of the uridylated mRNA body (Lim et al., 2014; Rissland and Norbury, 2009). Thus, the induction of TUT7 allows re-coupling of deadenylation and decay.

Although some mRNAs are uridylated and degraded almost immediately (Figure 7, left), the majority of maternal mRNAs undergo cytoplasmic polyadenylation, which delays uridylation and activates translation (Figure 7, middle). On the other hand, a minor but notable fraction of mRNAs is inherited with long poly(A) tails (Figure 7, right). These are translated almost immediately following fertilization and drive early events of zygotic gene expression. Conversely, these long-tailed mRNAs are also eventually deadenylated, uridylated, and degraded in due course during the MZT. Failure of maternal RNA clearance leads to poorly coordinated gene expression (Edgar and O'Farrell, 1990; Foe, 1989) and insufficient removal of inhibitory factors (Benoit et al., 2009; Collart et al., 2013; Edgar and Datar, 1996), resulting

in unsuccessful reprogramming of the genetic circuit (Giraldez, 2010). Maternal mRNA degradation appears to be temporally coordinated with cell-cycle remodeling and cell movement commencement (Tadros and Lipshitz, 2009; Walser and Lipshitz, 2011). In both zebrafish and *Xenopus*, we found that blockage of TUT7 translation results in developmental defects during gastrulation. The uridylation-defective embryos fail to phase out deadenylated transcripts and to achieve normal levels of later-stage zygotic transcription. Thus, uridylation facilitates transcriptome reprogramming, which in turn drives the developmental transition in early embryos.

Our TAIL-seq analyses provide the detailed landscape of mRNA tails during embryogenesis. Two critical features of RNA tail determine the fate of mRNA. First, the length of the poly(A) tail dictates the rate and timing of translation in the pre-MZT embryo as previously noted (Subtelny et al., 2014; Weill et al., 2012). Poly(A) tails of maternal transcripts undergo a dramatic remodeling via lengthening or shortening (Figure 7). Specifically, we found that maternal mRNAs related to very early embryonic functions, such as *nanog* and *pou5f3*, are deposited with long poly(A) tails that allow translational activation soon after fertilization. Nanog and Pou5f3 were previously shown to directly activate the first wave of zygotic transcription (Lee et al., 2013). The second key feature of mRNA tails, the oligo(U) tail, is coupled with the poly(A) tail status. Along with previous reports (Lim et al., 2014; Morgan et al., 2017), our study shows that TUT4/7 act selectively on short poly(A) tails and actuate the decay of deadenylated mRNAs. Thus, specificity of uridylation is conferred mainly by poly(A) length (Figure 7). Currently, it is not entirely clear how poly(A) length is controlled in a gene-specific manner during early embryogenesis. We have not been able to find a dominating motif common to the uridylated transcripts. This suggests that a combinatorial code of multiple *cis*-regulatory elements and *trans*-acting factors may control poly(A) shortening of maternal mRNAs (Belloc et al., 2008; Piqué et al., 2008), which in turn induce uridylation. Multiple factors, including miR-430, Smaug, Pumilio, EDEN-BP, codon optimality, 3′ UTR length, and m6A, have been reported to stimulate deadenylation of different subsets of maternal mRNAs (Bazzini et al., 2016; Heyn et al., 2014; Ivanova et al., 2017; Mishima and Tomari, 2016; Yartseva and Giraldez, 2015; Zhao et al., 2017). We find that TUT4/7 influence a wider range of maternal RNAs than any single factor among these regulators. Both maternal and zygotic modes of RNA degradation are dependent on TUT4/7 (Figure S7E). Given the specificity toward deadenylated mRNAs, TUT4/7 may serve as common downstream factors for these deadenylation inducers.

Uridylation has been shown to be involved in diverse RNA pathways in eukaryotes (Aphasizhev et al., 2016; Scheer et al., 2016; Scott and Norbury, 2013). Some precursors of miRNAs are uridylated, which leads to either degradation or DICER processing depending on the terminal structure of the precursor (Hagan et al., 2009; Heo et al., 2009; Jones et al., 2009; Lehrbach et al., 2009). This contributes to the context-dependent differential regulation of the let-7 miRNA family (Heo et al., 2012; Kim et al., 2015). Uridylation-mediated decay also serves as a cytosolic surveillance pathway for defective noncoding RNAs in *Drosophila*, mouse, and human cells (Pirouz et al., 2016; Reimão-Pinto et al., 2016; Ustianenko et al., 2016). Recently, uridylation by TUT4/7 was shown to play a crucial role during mouse oogenesis where it promotes the selective degradation of unneeded transcripts (Morgan et al., 2017). Our study is in line with these observations in that uridylation facilitates the temporally organized removal of unnecessary transcripts. This function appears to be particularly important during the rapid developmental transition such as oogenesis and embryogenesis in which the entire gene regulation network undergoes extensive remodeling.

During the amazing journey from an immature oocyte to a post-MZT embryo, TUT4/7 (particularly TUT7) enable stepwise termination of the "submodules" of the maternal program following the steps specified by several distinct deadenylation machineries. Our data show that, in zebrafish and *Xenopus*, the OXPHOS system and mitochondrial ribosome are suppressed by TUT4/7-driven decay at the earliest timing. Subsequently, TNF receptor superfamily binding proteins and calmodulin-dependent protein kinases are most significantly targeted. Uridylation-mediated RNA degradation reinforces the spatiotemporal organization of gene expression within the rapidly changing transcriptome of early life.

STAR★METHODS

Detailed methods are provided in the online version of this paper and include the following:

- KEY RESOURCES TABLE
- CONTACT FOR REAGENT AND RESOURCE SHARING
- EXPERIMENTAL MODEL AND SUBJECT DETAILS
  - Zebrafish embryos
  - *X. laevis* embryos
  - Mouse embryos
  - *D. melanogaster* embryos
- METHOD DETAILS
  - Embryo collection
  - Construction of TAIL-seq library
  - Plasmid construction
  - Microinjection
  - Genome reference databases and correction of genome assembly and gene annotations
  - Phylogenetic analysis of eukaryotic non-canonical terminal nucleotidyl transferases
  - Data processing of RNA-seq, ribo-seq datasets
  - Unsupervised clustering of gene expression patterns
  - Integrated analysis of TAIL-seq tags between two samples from different batches
- QUANTIFICATION AND STATISTICAL ANALYSIS
  - Data sources of analyses in the text and figures
  - Statistical analysis of mRNA abundance changes
  - Gene ontology analysis to find gene sets affected by TUT4/7 depletion
- DATA AND SOFTWARE AVAILABILITY

SUPPLEMENTAL INFORMATION

Supplemental Information includes seven figures and two tables and can be found with this article online at https://doi.org/10.1016/j.molcel.2018.03.004.

ACKNOWLEDGMENTS

We are grateful to the members of the Narry Kim lab for critical comments and helpful discussions. This research was supported by IBS-R008-D1 of the Institute for Basic Science from the Ministry of Science and ICT.

AUTHOR CONTRIBUTIONS

Conceptualization, V.N.K., H.C., and J.Y.; Methodology, H.C., J.L., and M.L.; Software, H.C.; Validation, J.Y. and H.K.; Formal Analysis, H.C.; Investigation, J.Y., H.C., H.K., J.K., M.L., H.H.K., J.L., J.O., and H.-Y.J.; Writing – Original Draft, J.Y. and H.C.; Writing – Review & Editing, V.N.K., H.C., and J.Y.; Visualization, H.C.; Supervision, V.N.K., K.-W.K., H.J., and H.L.; Project Administration, V.N.K.; Funding Acquisition, V.N.K., K.-W.K., H.J., and H.L.

DECLARATION OF INTERESTS

The authors declare no competing interests.

Received: December 5, 2017
Revised: February 7, 2018
Accepted: March 1, 2018
Published: April 5, 2018

SUPPORTING CITATIONS

The following citations appear in the Supplemental Information: Howe et al., 2013; Kanehisa et al., 2016; Le and Gascuel, 2008; Minasaki and Eckmann, 2012.

REFERENCES

Altschul, S.F., Gish, W., Miller, W., Myers, E.W., and Lipman, D.J. (1990). Basic local alignment search tool. J Mol Biol. *215*, 403–410.

Aphasizhev, R., Suematsu, T., Zhang, L., and Aphasizheva, I. (2016). Constructive edge of uridylation-induced RNA degradation. RNA Biol. *13*, 1078–1083.

Barckmann, B., and Simonelig, M. (2013). Control of maternal mRNA stability in germ cells and early embryos. Biochim. Biophys. Acta *1829*, 714–724.

Bazzini, A.A., Lee, M.T., and Giraldez, A.J. (2012). Ribosome profiling shows that miR-430 reduces translation before causing mRNA decay in zebrafish. Science *336*, 233–237.

Bazzini, A.A., Del Viso, F., Moreno-Mateos, M.A., Johnstone, T.G., Vejnar, C.E., Qin, Y., Yao, J., Khokha, M.K., and Giraldez, A.J. (2016). Codon identity regulates mRNA stability and translation efficiency during the maternal-to-zygotic transition. EMBO J. *35*, 2087–2103.

Belloc, E., Piqué, M., and Méndez, R. (2008). Sequential waves of polyadenylation and deadenylation define a translation circuit that drives meiotic progression. Biochem. Soc. Trans. *36*, 665–670.

Benoit, B., He, C.H., Zhang, F., Votruba, S.M., Tadros, W., Westwood, J.T., Smibert, C.A., Lipshitz, H.D., and Theurkauf, W.E. (2009). An essential role for the RNA-binding protein Smaug during the Drosophila maternal-to-zygotic transition. Development *136*, 923–932.

Chang, H. (2017). Tailseeker 3.1.7: The pipeline for high-throughput RNA poly(A) length and 3′) length and 3and 3roughput RN Zenodo Published online September 8, 2017. 10.5281/zenodo.887547).

Chang, H., Lim, J., Ha, M., and Kim, V.N. (2014). TAIL-seq: Genome-wide determination of poly(A) tail length and 3′ end modifications. Mol. Cell *53*, 1044–1052.

Collart, C., Allen, G.E., Bradshaw, C.R., Smith, J.C., and Zegerman, P. (2013). Titration of four replication factors is essential for the Xenopus laevis midblastula transition. Science *341*, 893–896.

Dobin, A., Davis, C.A., Schlesinger, F., Drenkow, J., Zaleski, C., Jha, S., Batut, P., Chaisson, M., and Gingeras, T.R. (2013). STAR: ULTRAFAST universal RNA-seq aligner. Bioinformatics *29*, 15–21.

Duval, C., Bouvet, P., Omilli, F., Roghi, C., Dorel, C., LeGuellec, R., Paris, J., and Osborne, H.B. (1990). Stability of maternal mRNA in Xenopus embryos: Role of transcription and translation. Mol. Cell. Biol. *10*, 4123–4129.

Edgar, B.A., and Datar, S.A. (1996). Zygotic degradation of two maternal Cdc25 mRNAs terminates Drosophila's early cell cycle program. Genes Dev. *10*, 1966–1977.

Edgar, B.A., and O'Farrell, P.H. (1990). The three postblastoderm cell cycles of Drosophila embryogenesis are regulated in G2 by string. Cell *62*, 469–480.

Eichhorn, S.W., Subtelny, A.O., Kronja, I., Kwasnieski, J.C., Orr-Weaver, T.L., and Bartel, D.P. (2016). mRNA poly(A)-tail changes specified by deadenylation broadly reshape translation in Drosophila oocytes and early embryos. eLife. Published online July 30, 2016. https://doi.org/10.7554/eLife.16955.

Facucho-Oliveira, J.M., and St John, J.C. (2009). The relationship between pluripotency and mitochondrial DNA proliferation during early embryo development and embryonic stem cell differentiation. Stem Cell Rev. *5*, 140–158.

Foe, V.E. (1989). Mitotic domains reveal early commitment of cells in Drosophila embryos. Development *107*, 1–22.

Folmes, C.D., Dzeja, P.P., Nelson, T.J., and Terzic, A. (2012). Metabolic plasticity in stem cell homeostasis and differentiation. Cell Stem Cell *11*, 596–606.

Gertz, E.M., Yu, Y.K., Agarwala, R., Schäffer, A.A., and Altschul, S.F. (2006). Composition-based statistics and translated nucleotide searches: improving the TBLASTN module of BLAST. BMC Biol. *4*, 41.

Giraldez, A.J. (2010). microRNAs, the cell's Nepenthe: Clearing the past during the maternal-to-zygotic transition and cellular reprogramming. Curr. Opin. Genet. Dev. *20*, 369–375.

Giraldez, A.J., Mishima, Y., Rihel, J., Grocock, R.J., Van Dongen, S., Inoue, K., Enright, A.J., and Schier, A.F. (2006). Zebrafish MiR-430 promotes deadenylation and clearance of maternal mRNAs. Science *312*, 75–79.

Grabherr, M.G., Haas, B.J., Yassour, M., Levin, J.Z., Thompson, D.A., Amit, I., Adiconis, X., Fan, L., Raychowdhury, R., Zeng, Q., et al. (2011). Full-length transcriptome assembly from RNA-seq data without a reference genome. Nat. Biotechnol. *29*, 644–652.

Guindon, S., and Gascuel, O. (2003). A simple, fast, and accurate algorithm to estimate large phylogenies by maximum likelihood. Syst. Biol. *52*, 696–704.

Hagan, J.P., Piskounova, E., and Gregory, R.I. (2009). Lin28 recruits the TUTase Zcchc11 to inhibit let-7 maturation in mouse embryonic stem cells. Nat. Struct. Mol. Biol. *16*, 1021–1025.

Harvey, S.A., Sealy, I., Kettleborough, R., Fenyes, F., White, R., Stemple, D., and Smith, J.C. (2013). Identification of the zebrafish maternal and paternal transcriptomes. Development *140*, 2703–2710.

Heo, I., Joo, C., Kim, Y.K., Ha, M., Yoon, M.J., Cho, J., Yeom, K.H., Han, J., and Kim, V.N. (2009). TUT4 in concert with Lin28 suppresses microRNA biogenesis through pre-microRNA uridylation. Cell *138*, 696–708.

Heo, I., Ha, M., Lim, J., Yoon, M.J., Park, J.E., Kwon, S.C., Chang, H., and Kim, V.N. (2012). Mono-uridylation of pre-microRNA as a key step in the biogenesis of group II let-7 microRNAs. Cell *151*, 521–532.

Heyn, P., Kircher, M., Dahl, A., Kelso, J., Tomancak, P., Kalinka, A.T., and Neugebauer, K.M. (2014). The earliest transcribed zygotic genes are short, newly evolved, and different across species. Cell Rep. *6*, 285–292.

Houseley, J., and Tollervey, D. (2009). The many pathways of RNA degradation. Cell *136*, 763–776.

Howe, D.G., Bradford, Y.M., Conlin, T., Eagle, A.E., Fashena, D., Frazer, K., Knight, J., Mani, P., Martin, R., Moxon, S.A., et al. (2013). ZFIN, the Zebrafish Model Organism Database: Increased support for mutants and transgenics. Nucleic Acids Res. *41*, D854–D860.

Ivanova, I., Much, C., Di Giacomo, M., Azzi, C., Morgan, M., Moreira, P.N., Monahan, J., Carrieri, C., Enright, A.J., and O'Carroll, D. (2017). The RNA m6A reader YTHDF2 is essential for the post-transcriptional regulation of the maternal transcriptome and oocyte competence. Mol. Cell *67*, 1059–1067.

Jones, M.R., Quinton, L.J., Blahna, M.T., Neilson, J.R., Fu, S., Ivanov, A.R., Wolf, D.A., and Mizgerd, J.P. (2009). Zcchc11-dependent uridylation of microRNA directs cytokine expression. Nat. Cell Biol. *11*, 1157–1163.

Kampstra, P. (2008). Beanplot: A boxplot alternative for visual comparison of distributions. J. Stat. Software *28*, 9.

Kanehisa, M., Sato, Y., Kawashima, M., Furumichi, M., and Tanabe, M. (2016). KEGG as a reference resource for gene and protein annotation. Nucleic Acids Res. *44* (D1), D457–D462.

Kim, B., Ha, M., Loeff, L., Chang, H., Simanshu, D.K., Li, S., Fareh, M., Patel, D.J., Joo, C., and Kim, V.N. (2015). TUT7 controls the fate of precursor microRNAs by using three different uridylation mechanisms. EMBO J. *34*, 1801–1815.

Kimmel, C.B., Ballard, W.W., Kimmel, S.R., Ullmann, B., and Schilling, T.F. (1995). Stages of embryonic development of the zebrafish. Dev. Dyn. *203*, 253–310.

Lackey, P.E., Welch, J.D., and Marzluff, W.F. (2016). TUT7 catalyzes the uridylation of the 3′ end for rapid degradation of histone mRNA. RNA *22*, 1673–1688.

Lapointe, C.P., and Wickens, M. (2013). The nucleic acid-binding domain and translational repression activity of a Xenopus terminal uridylyl transferase. J. Biol. Chem. *288*, 20723–20733.

Le, S.Q., and Gascuel, O. (2008). An improved general amino acid replacement matrix. Mol. Biol. Evol. *25*, 1307–1320.

Lee, M.T., Bonneau, A.R., Takacs, C.M., Bazzini, A.A., DiVito, K.R., Fleming, E.S., and Giraldez, A.J. (2013). Nanog, Pou5f1 and SoxB1 activate zygotic gene expression during the maternal-to-zygotic transition. Nature *503*, 360–364.

Lehrbach, N.J., Armisen, J., Lightfoot, H.L., Murfitt, K.J., Bugaut, A., Balasubramanian, S., and Miska, E.A. (2009). LIN-28 and the poly(U) polymerase PUP-2 regulate let-7 microRNA processing in Caenorhabditis elegans. Nat. Struct. Mol. Biol. *16*, 1016–1020.

Li, B., and Dewey, C.N. (2011). RSEM: Accurate transcript quantification from RNA-seq data with or without a reference genome. BMC Bioinformatics *12*, 323.

Li, W., and Godzik, A. (2006). Cd-hit: A fast program for clustering and comparing large sets of protein or nucleotide sequences. Bioinformatics *22*, 1658–1659.

Lim, J., Ha, M., Chang, H., Kwon, S.C., Simanshu, D.K., Patel, D.J., and Kim, V.N. (2014). Uridylation by TUT4 and TUT7 marks mRNA for degradation. Cell *159*, 1365–1376.

Lim, J., Lee, M., Son, A., Chang, H., and Kim, V.N. (2016). mTAIL-seq reveals dynamic poly(A) tail regulation in oocyte-to-embryo development. Genes Dev. *30*, 1671–1682.

Marzluff, W.F., Wagner, E.J., and Duronio, R.J. (2008). Metabolism and regulation of canonical histone mRNAs: Life without a poly(A) tail. Nat. Rev. Genet. *9*, 843–854.

Minasaki, R., and Eckmann, C.R. (2012). Subcellular specialization of multifaceted 3'end modifying nucleotidyltransferases. Curr. Opin. Cell Biol. *24*, 314–322.

Mishima, Y., and Tomari, Y. (2016). Codon usage and 3′ UTR length determine maternal mRNA stability in zebrafish. Mol. Cell *61*, 874–885.

Morgan, M., Much, C., DiGiacomo, M., Azzi, C., Ivanova, I., Vitsios, D.M., Pistolic, J., Collier, P., Moreira, P.N., Benes, V., et al. (2017). mRNA 3′ uridylation and poly(A) tail length sculpt the mammalian maternal transcriptome. Nature *548*, 347–351.

Morozov, I.Y., Jones, M.G., Gould, P.D., Crome, V., Wilson, J.B., Hall, A.J., Rigden, D.J., and Caddick, M.X. (2012). mRNA 3′ tagging is induced by nonsense-mediated decay and promotes ribosome dissociation. Mol. Cell. Biol. *32*, 2585–2595.

Mullen, T.E., and Marzluff, W.F. (2008). Degradation of histone mRNA requires oligouridylation followed by decapping and simultaneous degradation of the mRNA both 5′ to 3′ and 3′ to 5′. Genes Dev. *22*, 50–65.

Nieuwkoop, P.D., and Faber, J. (1994). Normal Table of Xenopus laevis (Daudin): A Systematical and Chronological Survey of the Development from the Fertilized Egg till the End of Metamorphosis (Garland).

Ochi, H., and Chiba, K. (2016). Hormonal stimulation of starfish oocytes induces partial degradation of the 3′ termini of cyclin B mRNAs with oligo(U) tails, followed by poly(A) elongation. RNA *22*, 822–829.

Ott, L.E., McDowell, Z.T., Turner, P.M., Law, J.M., Adler, K.B., Yoder, J.A., and Jones, S.L. (2011). Two myristoylated alanine-rich C-kinase substrate (MARCKS) paralogs are required for normal development in zebrafish. Anat. Rec. (Hoboken) *294*, 1511–1524.

Pasquinelli, A.E., Reinhart, B.J., Slack, F., Martindale, M.Q., Kuroda, M.I., Maller, B., Hayward, D.C., Ball, E.E., Degnan, B., Müller, P., et al. (2000). Conservation of the sequence and temporal expression of let-7 heterochronic regulatory RNA. Nature *408*, 86–89.

Pedregosa, F., Varoquaux, G., Gramfort, A., Michel, V., Thirion, B., Grisel, O., Blondel, M., Prettenhofer, P., Weiss, R., Dubourg, V., et al. (2011). Scikit-learn: Machine learning in python. J Mach Learn Res. *12*, 2825–2830.

Pei, J., Kim, B.H., and Grishin, N.V. (2008). PROMALS3D: A tool for multiple protein sequence and structure alignments. Nucleic Acids Res. *36*, 2295–2300.

Peshkin, L., Wühr, M., Pearl, E., Haas, W., Freeman, R.M., Jr., Gerhart, J.C., Klein, A.M., Horb, M., Gygi, S.P., and Kirschner, M.W. (2015). On the relationship of protein and mrna dynamics in vertebrate embryonic development. Dev. Cell *35*, 383–394.

Piqué, M., López, J.M., Foissac, S., Guigó, R., and Méndez, R. (2008). A combinatorial code for CPE-mediated translational control. Cell *132*, 434–448.

Pirouz, M., Du, P., Munafò, M., and Gregory, R.I. (2016). Dis3l2-mediated decay is a quality control pathway for noncoding RNAs. Cell Rep. *16*, 1861–1873.

Prieto, D., and Zolessi, F.R. (2017). Functional diversification of the four MARCKS family members in zebrafish neural development. J. Exp. Zoolog. B Mol. Dev. Evol. *328*, 119–138.

Reimão-Pinto, M.M., Manzenreither, R.A., Burkard, T.R., Sledz, P., Jinek, M., Mechtler, K., and Ameres, S.L. (2016). Molecular basis for cytoplasmic RNA surveillance by uridylation-triggered decay in Drosophila. EMBO J. *35*, 2417–2434.

Rissland, O.S., and Norbury, C.J. (2009). Decapping is preceded by 3′ uridylation in a novel pathway of bulk mRNA turnover. Nat. Struct. Mol. Biol. *16*, 616–623.

Rissland, O.S., Mikulasova, A., and Norbury, C.J. (2007). Efficient RNA polyuridylation by noncanonical poly(A) polymerases. Mol. Cell. Biol. *27*, 3612–3624.

Risso, D., Ngai, J., Speed, T.P., and Dudoit, S. (2014). Normalization of RNA-seq data using factor analysis of control genes or samples. Nat. Biotechnol. *32*, 896–902.

Ritchie, M.E., Phipson, B., Wu, D., Hu, Y., Law, C.W., Shi, W., and Smyth, G.K. (2015). limma powers differential expression analyses for RNA-sequencing and microarray studies. Nucleic Acids Res. *43*, e47.

Robinson, M.D., and Oshlack, A. (2010). A scaling normalization method for differential expression analysis of RNA-seq data. Genome Biol. *11*, R25.

Scheer, H., Zuber, H., De Almeida, C., and Gagliardi, D. (2016). Uridylation earmarks mRNAs for degradation… and more. Trends Genet. *32*, 607–619.

Schmidt, M.J., West, S., and Norbury, C.J. (2011). The human cytoplasmic RNA terminal U-transferase ZCCHC11 targets histone mRNAs for degradation. RNA *17*, 39–44.

Scott, D.D., and Norbury, C.J. (2013). RNA decay via 3′ uridylation. Biochim. Biophys. Acta *1829*, 654–665.

Sement, F.M., Ferrier, E., Zuber, H., Merret, R., Alioua, M., Deragon, J.M., Bousquet-Antonelli, C., Lange, H., and Gagliardi, D. (2013). Uridylation prevents 3′ trimming of oligoadenylated mRNAs. Nucleic Acids Res. *41*, 7115–7127.

Sive, H.L., Grainger, R.M., and Harland, R.M. (2007). Xenopus laevis in vitro fertilization and natural mating methods. CSH Protoc. Published online May 1, 2007. 10.1101/pdb.prot4737.

Su, Y.Q., Sugiura, K., Woo, Y., Wigglesworth, K., Kamdar, S., Affourtit, J., and Eppig, J.J. (2007). Selective degradation of transcripts during meiotic maturation of mouse oocytes. Dev. Biol. *302*, 104–117.

Su, W., Slepenkov, S.V., Slevin, M.K., Lyons, S.M., Ziemniak, M., Kowalska, J., Darzynkiewicz, E., Jemielity, J., Marzluff, W.F., and Rhoads, R.E. (2013). mRNAs containing the histone 3′ stem-loop are degraded primarily by decapping mediated by oligouridylation of the 3′ end. RNA *19*, 1–16.

Subtelny, A.O., Eichhorn, S.W., Chen, G.R., Sive, H., and Bartel, D.P. (2014). Poly(A)-tail profiling reveals an embryonic switch in translational control. Nature *508*, 66–71.

Tadros, W., and Lipshitz, H.D. (2009). The maternal-to-zygotic transition: A play in two acts. Development *136*, 3033–3042.

Talavera, G., and Castresana, J. (2007). Improvement of phylogenies after removing divergent and ambiguously aligned blocks from protein sequence alignments. Syst. Biol. *56*, 564–577.

The UniProt Consortium (2017). UniProt: The universal protein knowledgebase. Nucleic Acids Res. *45* (D1), D158–D169.

Thornton, J.E., Du, P., Jing, L., Sjekloca, L., Lin, S., Grossi, E., Sliz, P., Zon, L.I., and Gregory, R.I. (2014). Selective microRNA uridylation by Zcchc6 (TUT7) and Zcchc11 (TUT4). Nucleic Acids Res. *42*, 11777–11791.

Ustianenko, D., Pasulka, J., Feketova, Z., Bednarik, L., Zigackova, D., Fortova, A., Zavolan, M., and Vanacova, S. (2016). TUT-DIS3L2 is a mammalian surveillance pathway for aberrant structured non-coding RNAs. EMBO J. *35*, 2179–2191.

Van Blerkom, J. (2011). Mitochondrial function in the human oocyte and embryo and their role in developmental competence. Mitochondrion *11*, 797–813.

Vitti, M., Di Emidio, G., Di Carlo, M., Carta, G., Antonosante, A., Artini, P.G., Cimini, A., Tatone, C., and Benedetti, E. (2016). Peroxisome proliferator-activated receptors in female reproduction and fertility. PPAR Res. *2016*, 4612306.

Wagner, G.P., Kin, K., and Lynch, V.J. (2012). Measurement of mRNA abundance using RNA-seq data: RPKM measure is inconsistent among samples. Theory Biosci. *131*, 281–285.

Walser, C.B., and Lipshitz, H.D. (2011). Transcript clearance during the maternal-to-zygotic transition. Curr. Opin. Genet. Dev. *21*, 431–443.

Webb, S.E., and Miller, A.L. (2000). Calcium signalling during zebrafish embryonic development. BioEssays *22*, 113–123.

Weill, L., Belloc, E., Bava, F.A., and Méndez, R. (2012). Translational control by changes in poly(A) tail length: Recycling mRNAs. Nat. Struct. Mol. Biol. *19*, 577–585.

Yartseva, V., and Giraldez, A.J. (2015). The maternal-to-zygotic transition during vertebrate development: A model for reprogramming. Curr. Top. Dev. Biol. *113*, 191–232.

Zhao, B.S., Wang, X., Beadell, A.V., Lu, Z., Shi, H., Kuuspalu, A., Ho, R.K., and He, C. (2017). m^6A-dependent maternal mRNA clearance facilitates zebrafish maternal-to-zygotic transition. Nature *542*, 475–478.

STAR★METHODS

KEY RESOURCES TABLE

REAGENT or RESOURCE	SOURCE	IDENTIFIER
Chemicals, Peptides, and Recombinant Proteins		
T4 RNA ligase 2 (truncated KQ)	NEB	Cat#M0373L
RNase T1	Ambion	Cat#AM2283
T4 RNA ligase 1	NEB	Cat#M0204L
Superscript III Reverse Transcriptase	Invitrogen	Cat#18080085
AP endonuclease 1	NEB	Cat#M0282L
Human chorionic gonadotropin (hCG)	Daesung Microbiological Labs.	N/A
Marc's Modified Ringer's (MMR)	*Unknown source*	
Progesterone	Sigma-Aldrich	Cat#P0130
Calcium ionophore A23187	Sigma-Aldrich	Cat#C7522
Critical Commercial Assays		
TRIzol reagent	Invitrogen	Cat#15596018
RNeasy MinElute column	QIAGEN	Cat#74204
Ribo-Zero Magnetic Gold kit	Epicentre	Cat#MRZH11124
Dynabeads M-280 Streptavidin	Invitrogen	Cat#112.06D
PhiX control library	Illumina	Cat#FC-110-3001
mMessage mMachine SP6	Ambion	Cat#AM1340
ERCC RNA Spike-In Mix	Ambion	Cat#4456739
MiSeq Reagent Kit v2 (300 cycle)	Illumina	Cat#ILMS-102-2002
TruSeq stranded total RNA library prep kit	Illumina	Cat#20020596
Deposited Data		
Zebrafish genome and annotations reference database	This paper	DOI:10.5281/zenodo.157175
Fruit fly genome and annotations reference database	This paper	DOI: 10.5281/zenodo.192528
Mouse genome and annotations reference database	This paper	DOI: 10.5281/zenodo.203939
Frog genome and annotations reference database	This paper	DOI: 10.5281/zenodo.205747
TAIL-seq data for *Xenopus laevis* oocytes and embryos in various conditions (internal ID: ms97)	This paper	DOI: 10.5281/zenodo.1049188
TAIL-seq data for early stage mouse embryos (internal ID: ms85)	This paper	DOI: 10.5281/zenodo.1049186
TAIL-seq data for *Xenopus laevis* embryos injected with TUT4 and/or TUT7 morpholinos (internal ID: ms123)	This paper	DOI: 10.5281/zenodo.1049282
TAIL-seq data for wild-type zebrafish embryos (internal ID: hs25)	This paper	DOI: 10.5281/zenodo.1049284
		DOI: 10.5281/zenodo.1049418
		DOI: 10.5281/zenodo.1049424
		DOI: 10.5281/zenodo.1050706
		DOI: 10.5281/zenodo.1050708
		DOI: 10.5281/zenodo.1050710
		DOI: 10.5281/zenodo.1052881
		DOI: 10.5281/zenodo.1052896
		DOI: 10.5281/zenodo.1052898
		DOI: 10.5281/zenodo.1052900
		DOI: 10.5281/zenodo.1053295

(*Continued on next page*)

Continued

REAGENT or RESOURCE	SOURCE	IDENTIFIER
TAIL-seq data for wild-type *Xenopus laevis* early embryos (internal ID: hs27)	This paper	DOI: 10.5281/zenodo.1053301
		DOI: 10.5281/zenodo.1053304
		DOI: 10.5281/zenodo.1059159
		DOI: 10.5281/zenodo.1059161
		DOI: 10.5281/zenodo.1059163
		DOI: 10.5281/zenodo.1064289
		DOI: 10.5281/zenodo.1064291
		DOI: 10.5281/zenodo.1064293
		DOI: 10.5281/zenodo.1064319
		DOI: 10.5281/zenodo.1064323
		DOI: 10.5281/zenodo.1064327
		DOI: 10.5281/zenodo.1064355
TAIL-seq data for zebrafish embryos injected with TUT4/7 morpholinos, 3/6 hpf (internal ID: hs31)	This paper	DOI: 10.5281/zenodo.1065024
		DOI: 10.5281/zenodo.1065026
		DOI: 10.5281/zenodo.1065076
		DOI: 10.5281/zenodo.1065078
		DOI: 10.5281/zenodo.1065080
		DOI: 10.5281/zenodo.1065117
		DOI: 10.5281/zenodo.1065119
		DOI: 10.5281/zenodo.1065122
		DOI: 10.5281/zenodo.1065316
		DOI: 10.5281/zenodo.1065318
TAIL-seq data for zebrafish embryos injected with TUT4/7 morpholinos, 4/6 hpf (internal ID: hs41)	This paper	DOI: 10.5281/zenodo.1065658
		DOI: 10.5281/zenodo.1065660
		DOI: 10.5281/zenodo.1065662
		DOI: 10.5281/zenodo.1066574
		DOI: 10.5281/zenodo.1066576
		DOI: 10.5281/zenodo.1066578
RNA-seq data for zebrafish embryos injected with TUT4/7 morpholinos, 2/4/6 hpf (internal ID: rs1a)	This paper	GEO: GSE111152
RNA-seq data for zebrafish embryos injected with TUT4/7 morpholinos, 3/6 hpf (internal ID: rs1b)	This paper	GEO: GSE111152
RNA-seq data for zebrafish embryos injected with TUT4/7 morpholinos, 2/3/5 hpf (internal ID: rs2)	This paper	GEO: GSE111152
Unprocessed microscopy images	This paper	https://doi.org/10.17632/tzc5wwczyg.1
Experimental Models: Organisms/Strains		
Zebrafish: AB	Zebrafish International Resource Center	
Xenopus laevis: J	Korean *Xenopus* Resource Center for Research	
Mouse: ICR	Macrogen Inc.	
Drosophila melanogaster	Bloomington *Drosophila* Stock Center	
Oligonucleotides		
Oligonucleotides for TAIL-seq library, see Table S1	IDT	
Morpholinos, see Table S2	Gene Tools	
Recombinant DNA		
Plasmid: pCS2+-GFP-drTUT4-half	This paper	
pCS2+-GFP-drTUT7-half	This paper	

(*Continued on next page*)

Continued

REAGENT or RESOURCE	SOURCE	IDENTIFIER
pCS2+-GFP-xTUT7-half	This paper	
pCS2+-GFP-DADA-xTUT7-half	This paper	
Software and Algorithms		
Tailseeker 3.1.7	This paper	DOI: 10.5281/zenodo.887546
Inchworm	Grabherr et al., 2011	https://github.com/trinityrnaseq/trinityrnaseq/wiki
BLAST, TBLASTN	Altschul et al., 1990; Gertz et al., 2006	ftp://ftp.ncbi.nlm.nih.gov/blast/executables/blast+/LATEST/
PROMALS3D	Pei et al., 2008	http://prodata.swmed.edu/promals3d/info/readme.html
Gblocks	Talavera and Castresana, 2007	http://molevol.cmima.csic.es/castresana/Gblocks.html
PhyML	Guindon and Gascuel, 2003	http://www.atgc-montpellier.fr/phyml/
FigTree	Not published	http://tree.bio.ed.ac.uk/software/figtree/
STAR	Dobin et al., 2013	https://github.com/alexdobin/STAR
RSEM	Li and Dewey, 2011	https://deweylab.github.io/RSEM/
RUVseq	Risso et al., 2014	https://bioconductor.org/packages/release/bioc/html/RUVSeq.html
Trimmed mean of M-values (TMM) normalization algorithm	Robinson and Oshlack, 2010	http://bioconductor.org/packages/release/bioc/html/edgeR.html
limma	Ritchie et al., 2015	http://bioconductor.org/packages/release/bioc/html/limma.html
scikit-learn	Pedregosa et al., 2011	http://scikit-learn.org/

CONTACT FOR REAGENT AND RESOURCE SHARING

Further information and requests for resources and reagents should be directed to and will be fulfilled by the Lead Contact, V. Narry Kim (narrykim@snu.ac.kr).

EXPERIMENTAL MODEL AND SUBJECT DETAILS

Zebrafish embryos

Tübingen wild-type zebrafish AB strain was obtained from the Zebrafish International Resource Center (Oregon, USA). Zebrafish embryos were obtained by the natural mating of wild-type AB strain and grown in embryo medium at 28.5°C. All zebrafish work was carried out in accordance with protocols approved by the Institutional Animal Care and Use Committee of Seoul National University.

X. laevis embryos

Xenopus laevis were obtained from Nasco (Wisconsin, USA) and the Korean *Xenopus* Resource Center for Research. Embryos of *X. laevis* were obtained as described in Sive et al. (2007). Human chorionic gonadotropin was injected into a female frog 12 hours before collecting eggs. The eggs were obtained in 1X Marc's Modified Ringer's (MMR) solution and *in vivo* fertilized using excised testes from a male frog. Experiments were carried out with protocols approved by Yonsei University College of Medicine Institutional Animal Care and Use Committees (Seoul, Korea).

Mouse embryos

Total RNAs from inbred ICR strain mouse embryos were purchased from Macrogen Inc.

D. melanogaster embryos

Fly line of wild-type was obtained from the Bloomington *Drosophila* Stock Center.

METHOD DETAILS

Embryo collection

Zebrafish embryos were staged according to standard morphological criteria (Kimmel et al., 1995). A total of 300 wild-type zebrafish embryos at each stage were collected for TAIL-seq libraries. TAIL-seq libraries of MO-injected embryos were prepared using 100 embryos for each treatment group. The fertilized embryos were staged according to Nieuwkoop and Faber stages (Nieuwkoop and Faber, 1994). Fly embryos were collected on grape juice plates for the designated time frame at 25°C.

Construction of TAIL-seq library

TAIL-seq libraries were prepared as previously described (Lim et al., 2014). Briefly, 30–80 μg of total RNA was extracted from zebrafish, frog, or fly embryos using TRIzol (Invitrogen), treated with DNase I (Takara), purified with RNeasy MinElute column (QIAGEN), and rRNA-depleted by using Ribo-Zero Gold kit (Epicenter). The RNAs were ligated to the biotinylated 3′ adaptor using T4 RNA ligase 2, truncated KQ (NEB), and partially digested by RNase T1 (Ambion). The ligated RNAs were precipitated with streptavidin beads (Invitrogen), phosphorylated at the 5′ end by T4 polynucleotide kinase (Takara) reaction, and subjected to size fractionation (500–1000 nt). The purified RNAs were ligated to the 5′ adaptor, reverse-transcribed, and amplified by PCR. mTAIL-seq libraries were also prepared as described previously (Lim et al., 2016). Total RNAs were extracted from mouse embryo samples using TRIzol reagent (Invitrogen), and ligated to the mixture of 3′ hairpin adaptors using T4 RNA ligase 2 (NEB) overnight. The ligated RNAs were partially digested by RNase T1 (Ambion) and precipitated with streptavidin beads (Invitrogen). 5′ phosphorylation (T4 PNK, Takara) and endonucleolytic cleavage reaction (APE1, NEB) were performed on beads. The eluted RNAs were gel purified (300–750 nt), ligated to 5′ adaptor, reverse-transcribed and amplified by PCR. The cDNA libraries were mixed with PhiX sequencing control v3 (Illumina) and spike-in mixture (Chang et al., 2014) and then sequenced by paired-end run (51+251 cycles) on Illumina MiSeq or HiSeq 2500. The spike-ins were synthesized by Integrated DNA technologies. Each spike-in DNA was amplified and gel-purified as in the TAIL-seq library construction.

Plasmid construction

The coding sequences of C-terminal region of zebrafish TUT4 (681–1257 aa) and TUT7 (641–1196 aa) were cloned into the EcoRI and XbaI sites in the pCS2+-GFP-C1 vector: pCS2+-GFP-drTUT4-half and pCS2+-GFP-drTUT7-half. The C-terminal coding region of *Xenopus laevis* TUT7 (887–1518 aa) was cloned into the EcoRI and XbaI sites in the pCS2+-GFP vector: pCS2+-GFP-xTUT7-half. The catalytically inactive *Xenopus* TUT7 was generated by PCR-directed mutagenesis: pCS2+-GFP-DADA-xTUT7-half. Point mutation was introduced at residues 770 and 772 (aspartate to alanine) in the conserved catalytic domain of *Xenopus laevis* TUT7 (Lapointe and Wickens, 2013). Capped mRNAs were synthesized from linearized plasmids using the mMessage mMachine SP6 kit (Ambion).

Microinjection

Morpholinos were provided by Gene Tools, LLC and are listed in Table S2. Approximately 1 nL of the solution containing morpholinos was injected into wild-type zebrafish embryos at 1-cell stage. One-cell stage *Xenopus* embryos were injected with 2 nL of morpholino solution. For the rescue experiments, each mRNA was mixed with the translation-blocking morpholinos or control morpholinos and injected into 1-cell stage embryos. 50 or 150 pg of in-vitro transcribed mRNAs were injected into 1-cell stage zebrafish or *Xenopus* embryos, respectively.

Genome reference databases and correction of genome assembly and gene annotations

All analyses and design of oligonucleotides were based on genome assemblies and references, the NCBI RefSeq GRCz10 release 104 for zebrafish, the DOE Joint Genome Institute (JGI) *Xenopus laevis* genome 9.1 and XenBase annotation set 1.8.3.2 for *Xenopus laevis* and GENCODE GRCm38.p4 release M9 for mouse. The zebrafish genome GRCz10 had assembly problems near both regions for *zcchc6* and *zcchc11*, which generate corrupted coding sequences for translations of both genes. We corrected the tiling path of the genome assembly by manually building de Bruijn graphs of 15-mer sequences from our pooled RNA-seq data. The corrected tiling paths were confirmed with sequences assembled using the inchworm contig assembler (Grabherr et al., 2011) and tblastn matches against human protein sequences UniProt: Q5TAX3 and Q5VYS8 which were retrieved from the UniProt database (The UniProt Consortium, 2017). We have reported the corrections to the Genome Reference Consortium for preparation of the newer GRCz11 assembly (ZG-7155 and ZG-7156), and they were reflected in the final release. Since most of our work was finalized before the GRCz11 release, our analyses work around the issues by aggregating fragmented genes for downstream statistics after initially mapping to the original genome. The genomic reference databases used for this study are available for downloading from the Zenodo accession numbers 157175, 203939, and 205747.

Phylogenetic analysis of eukaryotic non-canonical terminal nucleotidyl transferases

To find homologous proteins of known non-canonical terminal nucleotidyltransferases (Figure S3), we collected known protein sequences from multiple protein sequence databases. We downloaded the protein sequences from the WormBase (release WS260) for *C. elegans,* the NCBI RefSeq (release 106) for *D. rerio*, the FlyBase (release 6.17) for *D. melanogaster,* the UniProt (SwissProt and TrEMBL release 20170705) for *E. nidulans* and *H. sapiens,* the NCBI RefSeq (release 103) for *G. gallus,* the PomBase

(as of Aug 29, 2017) for *S. pombe,* the NCBI RefSeq (release 101) for *S. purpuratus,* the XenBase (JGI genome 9.1 revision 1.8.3.2) for *X. laevis.* The homologs for seven human TUTases (UniProt: Q9NVV4, Q6PIY7, Q8NDF8, Q5XG87, Q9H6E5, Q5TAX3, and Q5VYS8 from the UniProt), *S. pombe* Cid1p (Uniprot: O13833), and *C. elegans* CID-1 (UniProt: Q09409) were searched using NCBI BLAST 2.2.31 against the protein databases with word size 3 and E-value cut-off 0.001. The truncated zebrafish protein sequences translated from *zcchc6* and *zcchc11* genes were corrected using the major open reading frames from our corrected genome assembly as mentioned above. The redundant sequences (splicing isoforms and short chromosome transcripts in *X. laevis* for e.g.) were removed using cd-hit 4.7 (Li and Godzik, 2006) with options ''-c 0.85 -aL 0.2 -aS 0.5 -G 0.'' PROMALS3D (Pei et al., 2008) was used for the multiple sequence alignment of the non-redundant homolog sequences with the default options and no 3D structural guide. The excessively divergent regions in the alignment are removed using Gblocks 0.91b (Talavera and Castresana, 2007) with the minimum number of sequence for a flank position set as 30, the maximum number of contiguous nonconserved positions set as 30, and full gap positions allowed. The phylogenetic with the maximum estimated likelihood was searched using PhyML 20120412 (Guindon and Gascuel, 2003) with options ''-d aa -m LG –r_seed 1 –bootstrap 500 –search BEST –rand_start –n_rand_starts 30.'' The consensus tree was visualized using FigTree (http://tree.bio.ed.ac.uk/software/figtree/). The edges in the tree were rotated manually for better visual recognition while keeping the topology and edge lengths same as in the original tree.

Data processing of RNA-seq, ribo-seq datasets

Sequenced reads from RNA-seq data were mapped to one of the reference genomes (see a previous section for the details) above using STAR 2.5.3a (Dobin et al., 2013) via RSEM 2.1.31 (Li and Dewey, 2011). The gene-level quantifications were performed using RSEM with the default options for strand-specific and paired-end RNA-seq. The first set of our zebrafish RNA-seq libraries was between-sample normalized using RUV-seq 1.10.0 (Risso et al., 2014). The standard workflow suggested by RUV-seq did not work due to the global changes of maternal transcripts following the progression of embryogenesis. Instead, we first chose a subset of spike-in RNAs that have $\geq$ 256 ''expected counts'' of reads in at least 90% of samples. Then, the counts were normalized by the RUVg algorithm (k = 1). The geometric means of the normalized counts were used as size factors for the scale normalization of all other RNAs. The ERCC spike-in reads in our second RNA-seq dataset were too unreliable to be used as references. Even the raw read counts mappable to the reference spike-in sequences were significantly out of the linear correlations between any two samples. As a workaround, we picked the internal controls from the first set to find genes that express more than 500 normalized reads with $\leq$ 0.2 of the $\log_2$ largest difference between two samples. Fourteen genes satisfied the criteria to become a set of internal controls. The internal reference genes were used in place of spike-in RNAs for processing counts by the modified indirect RUVg approach.

The sequences from the ribo-seq libraries and related control samples were trimmed to 28 nucleotides to remove trailing 3′ sequences. The trimmed sequences were aligned to the genome using STAR with options ''–outFilterType BySJout –outFilterMultimapNmax 20 –alignSJoverhangMin 8 –alignSJDBoverhangMin 1 –outFilterMismatchNmax 999 –alignIntronMin 20 –alignIntronMax 1000000 –alignMatesGapMax 1000000.'' Alignments with mapping quality lower than three were filtered out to suppress multiple mappings. A gene was quantified by counting reads overlapping to the union of coding regions of all transcripts except the first 50 nucleotides of each coding frame. The raw read counts were converted to transcripts per million (TPM) (Wagner et al., 2012), and then normalized by trimmed mean of M-values (TMM) (Robinson and Oshlack, 2010).

Unsupervised clustering of gene expression patterns

Figure S1B presents genes by their expression patterns. The clustering was done using our abundance measurements from TAIL-seq experiments. Among all annotated genes, ones that are not reliably quantifiable with TAIL-seq were removed. The high variations for those genes come from hybridization-based subtraction (rRNA and mitochondrial rRNA), or PAGE size fractionation (snoRNA, snRNA, scaRNA, miRNA, tRNA, and mitochondrial tRNA). The total sequenced RNA tag counts were normalized into reads per million mapped reads (RPM) values. Since the early embryonic transcriptome undergoes global transformation by the degradation of maternal RNAs, it was not feasible to use general normalization strategies which typically assume that a certain fraction of genes does not change between samples. Then, we counted TAIL-seq tags for genes whose transcripts read more than at least 99 RPM in any sample. The genes were clustered by gene-level expression patterns with *k*-means clustering and hierarchical clustering within each *k*-means cluster. The first clustering by the *k*-means algorithm were done with RNA abundance changes (tag counts divided by the maximum of tag counts). The *k* value was determined by the elbow method. The data points with less than ten TAIL-seq tags to support a mean length are replaced with 0. In each cluster, members are clustered again by hierarchical clustering with Pearson correlation distances and complete pairwise linkage. The orders between two clusters are determined by the weighted sum of centroids (-3, -2, -1, 1, 2, 3 as weights for 0, 1, 2, 4, 6, 8 hpf samples, respectively).

Gene groups differentiated by the responses to TNT3A/3B depletion are shown in Figure 5B. For this analysis, we first selected top 500 most expressed protein-coding genes in control sample of 2 hpf embryos by normalized read count. Despite the use of the smaller number of genes, the overall result was visually very similar to the outcome using 5000 genes. We chose the smaller gene count to minimize data point losses in the heatmap with a small footprint in the formatted paper. The expression data were transformed to $\log_2$-scale then subtracted by the levels in control samples. The transformed data were hierarchically clustered with Pearson correlation distances and complete pairwise linkage. The color gradients for both Figures S1B and 5B were mapped using yeun's Open Color lime and orange (https://yeun.github.io/open-color/) with extension in the lower 40% of the numeric range. The darker ranges were extended by linearly extrapolating *L* values in the CIELAB color space.

Integrated analysis of TAIL-seq tags between two samples from different batches

Analysis of TUT4/7 morpholino effects during the zebrafish embryogenesis required many different time points to enable testing various hypotheses. However, a single batch of TAIL-seq experiments after morpholino injection to zebrafish embryos had a too limited capacity to support as many samples as needed. Moreover, the recovery efficiency of poly(A) tails with different lengths varied substantially between batches. For the comparisons between samples produced from separate batches of the experiment, we calculated weighted summarizations for some of the derived statistics. In preparing Figure S7A, we had to compare between 3 and 4 hpf samples, which were separately prepared. The two batches related those samples included samples with an identical experimental condition, control MO-treated 6 hpf. We adjusted poly(A) length distribution of one of the batch to the other using genes with at least 200 poly(A)$^+$ reads in all related libraries. Using the tags from those genes, we estimated the poly(A) length related bias factor with the median ratio between long ($\geq$20 nt) and short (< 20 nt) poly(A) tails. The fold change in each criterion in Figure S7A was calculated after correcting the long-short ratio variation. The size factor in each library was estimated the most stable and abundant genes as references. We sought the fifty candidate genes which had the smallest variance of the normalized sequence read counts in control MO-treated 2 hpf, control MO-treated 4 hpf, TUT4/7 MO-treated 2 hpf, and TUT4/7 MO-treated 4 hpf samples among the 5000 most expressed genes in control MO-treated 2 hpf sample. We excluded any gene which had less than fifty poly(A)$^+$ reads in all related TAIL-seq samples. With the remaining seventeen reference genes, we took the median offset to the median tag counts as a size adjustment factor for the linear scale normalization of a library.

QUANTIFICATION AND STATISTICAL ANALYSIS

Data sources of analyses in the text and figures

Quantitative analyses used in the text and figures are based on the experimental sources as specified in this section. The list of internal IDs of the datasets and their details are available in Key Resources Table.

- Figures 1B–1D: hs25, n = 1.
- Figure 1E: hs25, n = 1 (x axis); GEO: GSM1276545, GSM1276554 (Subtelny et al., 2014), n = 1 (y axis).
- Figure 2A: hs25, n = 1 (zebrafish); hs27, n = 1 *(X. laevis);* ms85, n = 1 (mouse).
- Figure 2B: hs25, n = 1.
- Figure 3A: hs31, n = 1 (3, 6 hpf); hs35, n = 1 (4 hpf); hs40, n = 1 (5 hpf).
- Figure 3B: ms97, n = 1.
- Figure 3C: hs25, n = 1.
- Figure 3D: GEO: GSM1276545, GSM1276554 (Subtelny et al., 2014), n = 1.
- Figure 4E: ms123, n = 1.
- Figure 5A: rs1a, n = 1 (2, 4, 6 hpf); rs1b, n = 1 (3, 6 hpf).
- Figures 5B–5D: rs1a, n = 1.
- Figure 6A: rs1a, n = 1 (4, 6 hpf, RNA abundance); hs40, n = 1 (5 hpf, uridylation).
- Figure 6B: hs25, n = 1 (x axis), rs1a, n = 1 (y axis).
- Figure 6C: hs25, n = 1 (zebrafish); hs27, n = 1 *(X. laevis);* ms85, n = 1 (mouse).
- Figure 6D: rs1a, n = 1.
- Figures 6E–6F: rs2, n = 1.
- Figures S1A, S1B, and S2A: hs25, n = 1.
- Figures S2B and S2C: ms97, n = 1.
- Figure S2D: ms49, n = 1.
- Figure S4B: ms97, n = 1.
- Figure S4C: hs40, n = 1.
- Figure S4D: http://kirschner.med.harvard.edu/XeXe.html (Peshkin et al., 2015), n = 1.
- Figure S5B: ms123, n = 1.
- Figures S6A and S6B: rs1a, n = 1.
- Figure S7A: hs41, n = 1 (4, 6 hpf), hs31, n = 1 (3, 6 hpf) — 6 hpf samples are used as a bridge to cancel out batch effects.
- Figure S7B: hs31, n = 1.
- Figure S7C: rs1a, n = 1 (2, 4, 6 hpf); rs2, n = 1 (3, 5 hpf).
- Figure S7D: rs2, n = 1.
- Figure S7E: rs1a, n = 1.

Statistical analysis of mRNA abundance changes

Principal component analysis (PCA) for Figure 5A was performed with top 5000 protein-coding genes by the peak expression level in any sample. The normalized expression levels were transformed to log-scale after adding one as pseudocount. The batch effect in the expression matrix was canceled out using removeBatchEffect in the limma package (Ritchie et al., 2015) to make the first two

principal components (PC1–2) directly interpretable. PCA for the matrix was done using the scikit-learn. Since the PC1 turned out to explain 83.14% of the variance and the resulting transform function also worked consistently for the other experiments (data not shown), we speculated that the PC1 was a good proxy for the developmental stage of a transcriptome.

To classify genes for miR-430 targeting analysis (Figure S7E), we used the data from the RNA-seq experiments by Mishima and Tomari (2016). First, we quantified the gene-level expressions as described above. A subset of maternal genes (included in clusters *a, b,* and *c* in Figure S1B) were selected for the classification when they were expressed more than 10 TPM on average in all 6 hpf control samples in Mishima and Tomari (2016) and 20 of a normalized read count in our 4 hpf control sample. A gene was regarded as a confident target of miR-430 if it was derepressed by no less than 50% on miR-430 antagomir treatment. Among the confident targets, we further classified into direct and indirect targets. A gene was classified as a direct miR-430 target if a 3′ UTR sequence of any annotated isoform contained at least one exact reverse complementary match to the miR-430 seed sequence. Genes which were included in cluster *e* were included as "stable genes" in the figure.

Gene ontology analysis to find gene sets affected by TUT4/7 depletion

The gene ontology (GO) associations in zebrafish were fairly insufficient and biased to well-studied functions and genes. To increase the sensitivity and coverage of our gene set analysis, we imported GO associations with weaker supports or less certain orthologs from other organisms. GO relationships and associations for zebrafish, human, mouse, and *X. laevis* were downloaded from the Gene Ontology Consortium on Nov 26, 2016. ZFIN IDs in the associations were converted to ENSEMBL IDs using the mapping table downloaded from the BioMart (Ensembl Genes 90). Ortholog mappings of zebrafish genes in human, mouse, and *X. laevis* were downloaded from the BioMart. All gene- and protein-based associations in those species were mapped to zebrafish genes via those orthologous relationships and gene-translation relationships defined in the ENSEMBL.

To search the gene sets that were affected by TUT4/7 depletion during the maternal-to-zygotic transition, we tested each GO term if the derepression levels of associated genes were statistically different from those of the other genes. The derepression level D of a gene is defined as

$$D = \log_2 \frac{T_5 + 1}{T_3 + 1} - \log_2 \frac{C_5 + 1}{C_3 + 1}$$

where C_t and T_t are the normalized read counts for t hpf sample of control and TUT4/7 morpholino-treated embryos, and 1 is added to each term as a pseudocount. Top 8000 genes by expression level in control 3 hpf sample were selected among all protein-coding genes except cell cycle-dependent histone mRNAs. For GO terms associated with ten or more selected genes, the derepression levels of the associated genes were tested against those of all other genes by two-sided Mann-Whitney U test. The p values were adjusted for multiple testing to produce false discovery rates (FDRs) by the Benjamini-Hochberg procedure. We filtered the test results with 5% FDR cut-off to produce the list of affected gene sets. For Figures 6D and 6E, the FDR-filtered list of affected gene sets was represented in order of Cohen's *d* for the $\log_2$ fold changes in control and TUT4/7-depleted embryos. We skipped a gene set if associated genes overlap by more than a half with those of another gene set that had a greater absolute effect size *(d)*. For the "less affected" gene sets, we selected gene sets having the minimum median absolute derepression levels of associated genes with at least fifteen member genes. The distributions are visualized using the beanplot package in R (Kampstra, 2008).

DATA AND SOFTWARE AVAILABILITY

All TAIL-seq data were processed with Tailseeker 3.1.7 (Chang, 2017) according to the standard workflow of the software. The source codes and container images are available from Zenodo (https://zenodo.org/record/887547; https://doi.org/10.5281/zenodo.887546), GitHub (https://github.com/hyeshik/tailseeker/), or DockerHub (https://hub.docker.com/r/hyeshik/tailseeker/).

All high-throughput sequencing data generated for this paper are deposited in Zenodo and unprocessed images are available at Mendeley Data. See Key Resources Table for the accessible locations.